Journal of Solid State Chemistry **154,** 476–482 (2000)
doi:10.1006/jssc.2000.8867, available online at http://www.idealibrary.com on IDEAL®

Semiconductor Sensitization by Microcrystals of $MgIn_2S_4$ on Wide Bandgap $MgIn_2O_4$

Prasad Manjusri Sirimanne, Noriyuki Sonoyama, and Tadayoshi Sakata[1]

Department of Electronic Chemistry, Interdisciplinary Graduate School of Science and Engineering, Tokyo Institute of Technology, 4259 Nagatsuta, Midori-ku, Yokohama 226-8502, Japan

Received March 27, 2000; in revised form June 15, 2000; accepted July 13, 2000; published online September 30, 2000

$MgIn_2O_4$ was prepared by the solid state reaction of MgO and In_2O_3. Microcrystals of $MgIn_2S_4$ were formed on sintered $MgIn_2O_4$ pellets by sulfurizing them in a H_2S atmosphere. The bandgap of $MgIn_2S_4$ was evaluated as 2.1 eV. A very high efficiency photocurrent was observed on $MgIn_2S_4|MgIn_2O_4$ electrodes. Photocurrent generation of $MgIn_2S_4|MgIn_2O_4$ electrodes was explained from the viewpoint of semiconductor sensitization. The flat band potential of $MgIn_2S_4$ was evaluated as -1.0 V vs Ag|AgCl in aqueous polysulfide redox electrolyte (1 M OH^-, 1 M S^{2-}, 10^{-2} M S). © 2000 Academic Press

Key Words: **$MgIn_2O_4$; $MgIn_2S_4$; sulfurization; semiconductor sensitization.**

1. INTRODUCTION

During the past years, utilization of photovoltaic cells as a power source in various fields has shown tremendous growth. In this viewpoint, the contribution of semiconductor electrodes is significant. Photoelectrochemical behaviors of many *n*-type semiconductors have been extensively investigated. In recent years, considerable interest has been focused on spectral sensitization of wide bandgap semiconductors by inorganic complexes (1–3). Semiconductor sensitization is another method of extending the photoresponse of wide bandgap materials to longer wavelength regions. Such multicomponent semiconductor electrodes exhibit a wide range of novel electric and photoelectrochemical properties (4–7). Semiconductor sensitization takes place only when the following conditions are satisfied by two components of the compound electrodes. The edge of the conduction band of light harvesting material of the compound electrodes must be more negative than the conduction band of the substrate which accepts photogenerated electrons. The energy difference between two semiconductor systems must be significant to prevent recombination of the charge carriers and reverse flow of electrons. However, long-term stability of these sensitizing materials under different photoelectrochemical conditions was one of the most important problems observed in previous studies. Sulfurization of surfaces of metal oxide electrodes is a very simple and useful technique for designing semiconductor hetero structures or multicomponent semiconductor electrodes. We have succeeded in preparing $MgIn_2S_4$ by sulfurizing $MgIn_2O_4$ pellets in a H_2S atmosphere. $MgIn_2O_4$ and $MgIn_2S_4$ are members of the ternary compound with common formula of AB_2X_4 family whose structure and physical properties have been thoroughly studied in recent years. In the lattice, $MgIn_2S_4$ crystallizes in spinel structure with lattice parameter $a = 10.7108$ Å and deformation parameter $u = 0.383$. The distribution of cations in the unit cell of $MgIn_2S_4$ is $Mg^{2+}_{0.16}In^{3+}_{0.84}[Mg^{2+}_{0.84}In^{3+}_{1.16}]$, where the ions in brackets occupy octahedral sites and the remaining cations are occupied in tetrahedral sites (8,9). $MgIn_2O_4$ is a binary oxide of MgO and In_2O_3 with inverted spinel structure. The distribution of In^{3+} and Mg^{2+} cations in tetrahedral and octahedral sites was confirmed from Rietveld analysis (10). In the unit cell, two tetrahedral sites are occupied by In^{3+} and four octahedral sites are randomly occupied by In^{3+} and Mg^{2+} (10). In the past three decades, not much attention has been paid to photoelectrochemical studies of ternary compounds with common formula AB_2X_4. As far as we know, optical and photoelectrochemical properties of $MgIn_2S_4$ have not been studied yet. We studied the capability of $MgIn_2S_4|MgIn_2O_4$ electrodes as electrodes for harvesting light in photoelectrochemical (PEC) cells. In the present article, we report our primary observations of $MgIn_2S_4|MgIn_2O_4$ electrodes. Photocurrent generation of $MgIn_2S_4|MgIn_2O_4$ electrodes is described from the viewpoint of semiconductor sensitization.

2. EXPERIMENTAL

2.1. Preparation of $MgIn_2O_4$ and $MgIn_2S_4|MgIn_2O_4$ Pellets

The chemicals used in the present study were of the highest available purity and as purchased from the

[1]To whom corresondence should be addressed. Fax: + 81 45 924 5489. E-mail: sakata@echem.titech.ac.jp.

0022-4596/00 $35.00

suppliers. Double distilled water was used to prepare the electrolyte. $MgIn_2O_4$ was prepared from the solid state reaction of MgO (Kanto Chemical Co. 99.99%) and In_2O_3 (Kanto Chemical Co. 99.9%) using two different methods.

Method I. MgO and In_2O_3 were mixed in a Mg/In ratio slightly greater than 0.5 by wet ball milling with methanol and allowed to dry in a fume chamber. $MgIn_2O_4$ was prepared by calcining the mixture of MgO and In_2O_3 in an Al_2O_3 crucible at 1350°C for 10 h in air. Excess MgO was removed from the heated materials by dispersing in 1 M NH_4Cl at 100°C for several hours, following ball-milling heated materials with methanol. The residual was then rinsed several times with distilled water to remove excess NH_4Cl. The pure wet powder sample of $MgIn_2O_4$ was dried in a vacuum oven at 150°C for several hours.

Method II. MgO and In_2O_3 were mixed in a one-to-one molar mixture of MgO and In_2O_3 by wet ball milling. $MgIn_2O_4$ was prepared by repeating the sintering process until the X-ray difractrogram showed single-phase $MgIn_2O_4$. The temperature of the furnace was maintained at 1350°C.

Sintered $MgIn_2O_4$ pellets were prepared by heating compressed powder pellets at 1400°C for 10 h in air. Microcrystals of $MgIn_2S_4$ were formed on sintered $MgIn_2O_4$ pellets by sulfurizing them at 700°C for several minutes in a H_2S atmosphere. The sulfurization was carried out in a tube furnace and H_2S gas was passed at a constant rate of 0.5 ml/min throughout the sulfurization.

2.2. *Characterization and Analysis of $MgIn_2O_4$ and $MgIn_2S_4|MgIn_2O_4$ Electrodes*

Scanning electron micrographs and X-ray diffractograms of sintered $MgIn_2O_4$ and $MgIn_2S_4|MgIn_2O_4$ pellets were obtained using a scanning electron spectrometer (Jeol, JSM-5600) and an X-ray diffractometer (Rigaku, RINT-2100). Diffuse reflectance spectra of sintered $MgIn_2O_4$ and $MgIn_2S_4|MgIn_2O_4$ pellets were obtained using a UV–Vis scanning spectrometer coupled with an integrating sphere (Shimadzu, UV-2100 PC) and were converted to absorption spectra by using the Kubelka-Munk equation.

2.3. *Photoelectrochemical Measurements*

Ga–In alloy was used to make ohmic contact of the back side of the pellet with copper wire; the back side of the pellet was covered with an epoxy layer. Photoelectrochemical measurements were carried out with a standard two-compartment cell consisting of a Pt wire gauze as the counterelectrode and a Ag|AgCl electrode as the reference electrode. Current–voltage characteristics of the electrodes were obtained by measuring current across the working electrode and the counterelectrode under chopped white light illumination. The potential of the working electrode was scanned with respect to the reference electrode from $+0.60$ to -1.2 V. Stability of the photocurrent was studied by applying a constant voltage of $+200$ mV vs Ag|AgCl on the working electrode. A potensiostat–galvanostat (Hokuto Dento, HABF-501) coupled with a computer (NEC, PE-9801 UV) and a collimated beam from a 500-W Xe lamp (Ushio Electric Instruments, UI 501C) were used to measure steady-state photocurrent and current–voltage characteristics. Photocurrent action spectra were measured by exciting the working electrodes with monochromatic light. An aqueous solution of 1 M OH^-, 1 M S^{2-}, and 10^{-2} M S was used as the electrolyte. Light intensity was measured with a thermophile (The Eppley Laboratory, Inc.).

3. RESULTS AND DISCUSSION

3.1. *General Properties of $MgIn_2O_4$ and $MgIn_2S_4|MgIn_2O_4$ Electrodes*

$MgIn_2O_4$ prepared from the solid state reaction of MgO and In_2O_3 using two different methods exhibited similar structural and photoelectrochemical behavior. $MgIn_2O_4$ powder was white in color and exhibited insulator properties. Sintered $MgIn_2O_4$ pellets were slightly bluish white and exhibited a high degree of hardness and low electric resistivity ($< 5\ \Omega$ cm) at room temperature. The low electric resistivity on sintered $MgIn_2O_4$ pellets may be due to O_2 defects produced during sintering at high temperature (11,12). Most compounds represented by the common formula AB_2O_4 show a solid solution with other B_2O_3-type oxides in the lattice (13). We did not observe any evidence of solubility of In_2O_3 in $MgIn_2O_4$ for the samples prepared as described in this article. The X-ray diffractogram reveals that $MgIn_2O_4$ is composed of a single phase and agrees with that of JCPDS data (Card 40-1402). As we expected, sulfurization is considered to form $MgIn_2S_4$ on sintered $MgIn_2O_4$ pellets via the following chemical reaction:

$$MgIn_2O_4 + 4H_2S \rightarrow MgIn_2S_4 + 4H_2O. \qquad [1]$$

Yellowish dark brown coloration manifests the formation of $MgIn_2S_4$, which was confirmed by X-ray diffraction measurements. An X-ray diffractogram of a sulfurized $MgIn_2O_4$ pellet is shown in Fig. 1. Sharp diffraction lines indicate that $MgIn_2O_4$ and $MgIn_2S_4|MgIn_2O_4$ pellets have a high degree of crystallinity. A scanning electron micrograph of a sintered $MgIn_2O_4$ pellet after and before sulfurization is shown in Fig. 2. As is shown in this figure, scanning electron micrography (Fig. 2a) indicates clearly that sintered $MgIn_2O_4$ pellets are highly porous. It has been reported that the density of such porous sintered $MgIn_2O_4$ pellets is less than that of single crystals (12). Small round bright

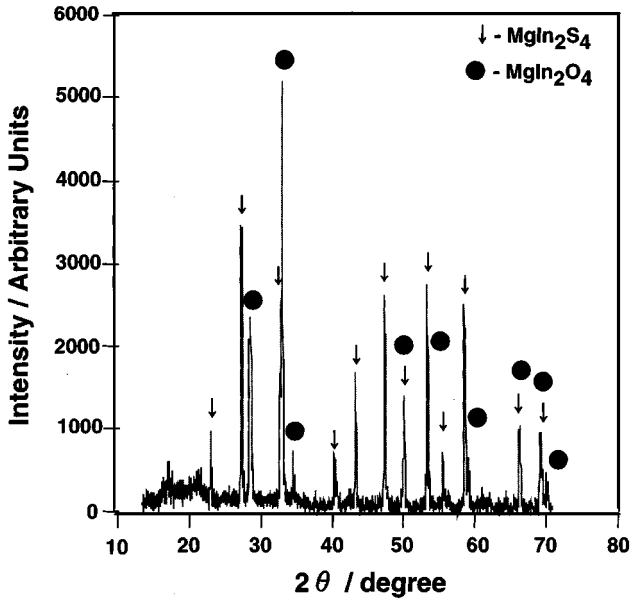

FIG. 1. X-ray diffractogram of sulfurized $MgIn_2O_4$ pellet.

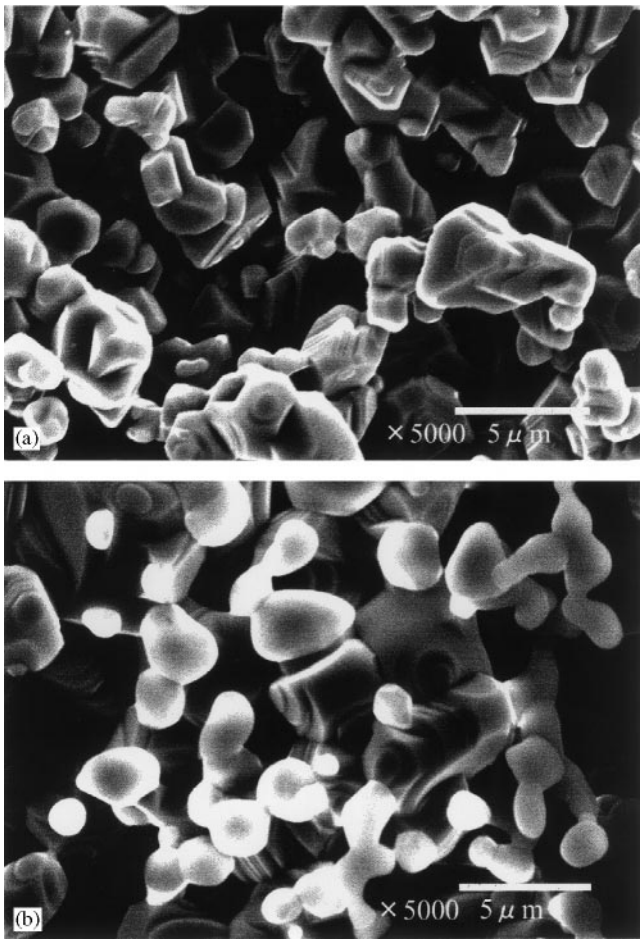

FIG. 2. Scanning electron micrograph of sintered $MgIn_2O_4$ pellet (a) before and (b) after sulfurization.

grains in Fig. 2b seem to be $MgIn_2S_4$ microcrystals of about 1 μm radius and large grains are $MgIn_2O_4$. This figure indicates that the $MgIn_2S_4$ thin film formed on the $MgIn_2O_4$ pellet is composed of microcrystals. The cluster size of $MgIn_2S_4$ and the thickness of the $MgIn_2S_4$ film can easily be controlled by varying the sulfurization time or the temperature of the furnace. An absorption spectrum of a sintered $MgIn_2O_4$ pellet after and before sulfurization is shown in Fig. 3, the onset of absorption is around 400 nm. Growth of $MgIn_2S_4$ on $MgIn_2O_4$ shifted the onset of absorption of sulfurized samples to a longer wavelength region than in the nonsulfurized sample. The onset of absorption of $MgIn_2S_4$| $MgIn_2O_4$ pellets is around 650 nm. Bandgap energies of $MgIn_2O_4$ and $MgIn_2S_4$ were evaluated by analyzing an $(Ah\nu)^2$ vs $h\nu$ plot for the same samples, where A is the absorbance, h is the planck constant, and ν is the frequency. The direct bandgap energy of $MgIn_2O_4$ evaluated by this method is about 3.2 eV. The evaluated bandgap energy for $MgIn_2O_4$ in the present work deviates slightly from 3.4 eV, as reported by Kawazoe *et al.* (10). The observed shift in the onset of absorption and bandgap of $MgIn_2O_4$ might be attributed to random localization of In^{3+} and Mg^{2+} cations in octahedral sites in the unit cell, substituted cations, doping of foreign atoms in interstitial sites, and a slight difference in chemical composition (10,14,15). The bandgap energy of $MgIn_2S_4$ was evaluated as 2.1 eV. Goodenough *et al.* maintained that the electronegativity difference between cations and anions (E_M–E_I) is responsible for the bandgap of a material, and replacement of oxygen atoms with sulfur atoms decreases the electronegativity difference between cations and anions in host material (16). Replacement of oxygen atoms by sulfur atoms in $MgIn_2O_4$ lattice might be one reason a much smaller bandgap was observed for $MgIn_2S_4$ than for $MgIn_2O_4$.

3.2. Photoelectrochemical Behavior of $MgIn_2O_4$ and $MgIn_2S_4$|$MgIn_2O_4$ Electrodes

The current–voltage curve of an $MgIn_2O_4$ electrode before and after sulfurization is shown in Fig. 4. When the electrode potential was swept toward the anodic potential, only weak anodic current was observed, whereas under cathodic polarization, a sudden rise of cathodic current was observed at -1.5 V vs Ag|AgCl on $MgIn_2O_4$ electrode, in the dark, as is shown in Fig. 4a. This behavior indicates that $MgIn_2O_4$ is an *n*-type semiconductor. When the potential of the $MgIn_2O_4$ electrode was further negatively swept from -1.5 V vs Ag|AgCl, a color change was observed on the electrode surface because of reduction of $MgIn_2O_4$. This metallic color might be attributed to In metal produced by

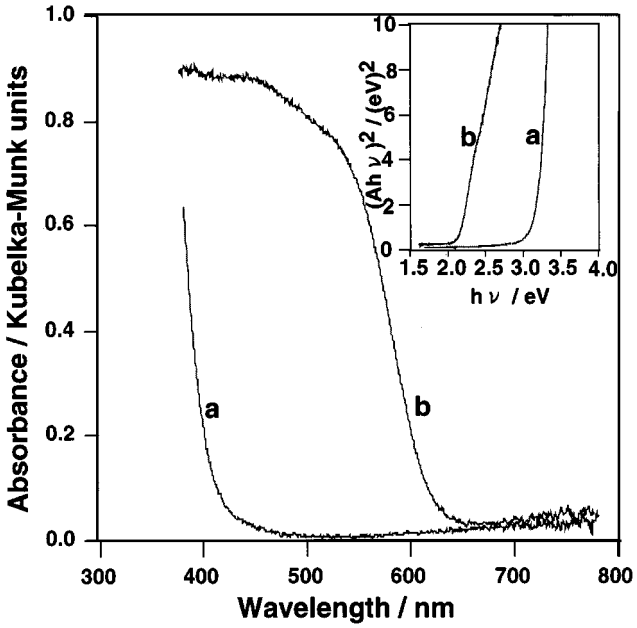

FIG. 3. Normalized absorption spectrum of sintered $MgIn_2O_4$ pellet (a) before and (b) after sulfurization. (Inset) Variation of $(Ahv)^2$ vs photon energy of sintered $MgIn_2O_4$ pellet (a) before and (b) after sulfurization.

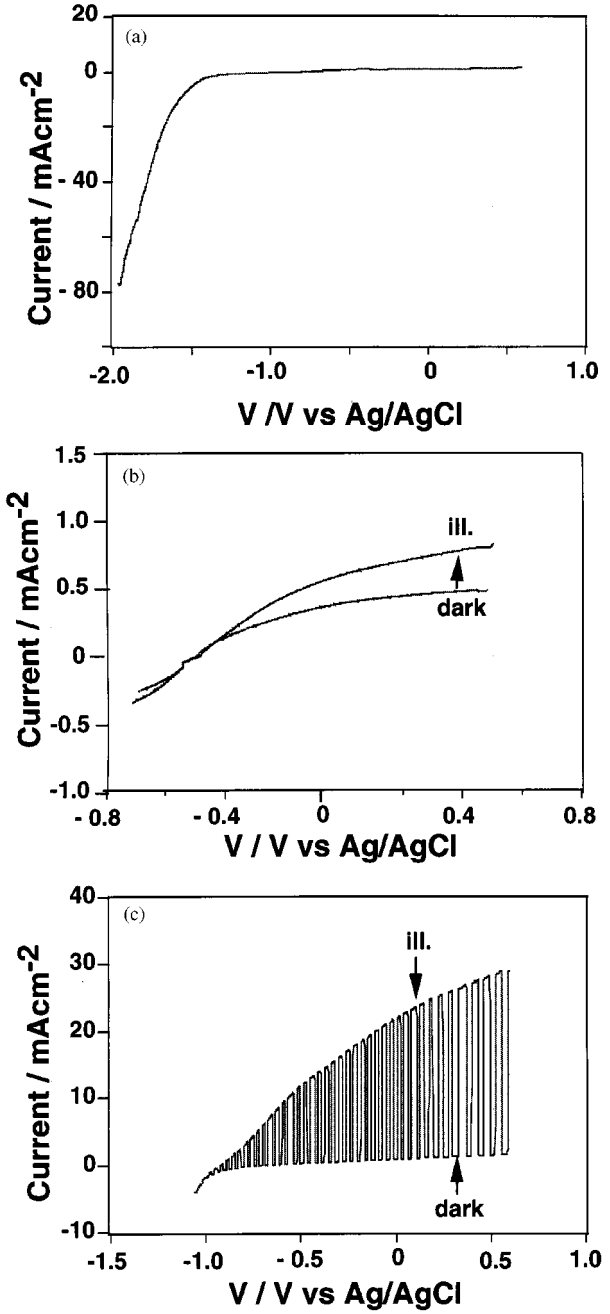

FIG. 4. Current–voltage curve of Pt|polysulfide|$MgIn_2O_4$ cell (a) in the dark and (b) under illumination and (c) current–voltage curve of Pt|polysulfide|$MgIn_2S_4$|$MgIn_2O_4$ cell. Scan rate was 10 mV/s. Polychromatic light (250 mW cm^{-2}) from a Xe lamp was used as the light source. In the case of Pt|polysulfide|$MgIn_2S_4$|$MgIn_2O_4$ PEC cell incident light was manually chopped by introducing a thick metal sheet into light path.

reduction of In^{3+} in $MgIn_2O_4$ under strong cathodic polarization. $MgIn_2O_4$ electrodes exhibited weak anodic photoresponse in the UV region. Figure 4b represents a magnified current–voltage curve of the $MgIn_2O_4$ electrode under illumination and in the dark in the photoresponse potential region. The current–voltage curve of a sulfurized $MgIn_2O_4$ electrode under polychromatic illumination is shown in Fig. 4c. As is shown in this figure, anodic photocurrent was observed on sulfurized $MgIn_2O_4$ electrodes. This anodic photocurrent increased with increasing anodic potential. This behavior indicates that $MgIn_2S_4$|$MgIn_2O_4$ electrodes also behave as *n*-type semiconductors (17). Current–voltage curves give a qualitative estimate of the flat band potential of semiconductors. In the present study, the flat band potentials of $MgIn_2O_4$ and $MgIn_2S_4$|$MgIn_2O_4$ electrodes are determined as -0.55 and -1.0 V vs Ag|AgCl, respectively, in 1 M OH^-, 1 M S^{2-}, 10^{-2} M S. The energy diagram of $MgIn_2S_4$|$MgIn_2O_4$ electrodes is written by taking into account flat band potentials and bandgap values of both materials. The energy difference between the conduction band of $MgIn_2S_4$ and that of $MgIn_2O_4$ is estimated as 0.45 eV from the difference in their flat band potentials. Proposed charge generation and separation of $MgIn_2S_4$|$MgIn_2O_4$ electrodes under illumination is illustrated schematically in Fig. 5. Charge generation and separation of $MgIn_2S_4$|$MgIn_2O_4$ electrodes under illumination can be summarized by the following equations,

Excitation of the $MgIn_2S_4$ layer,

$$MgIn_2S_4 + hv \rightarrow MgIn_2S_4(e - h), \qquad [2]$$

Photoinduced electron injection to the conduction band of $MgIn_2O_4$,

$$MgIn_2S_4(e - h) \rightarrow MgIn_2S_4(h) + MgIn_2O_4(e). \qquad [3]$$

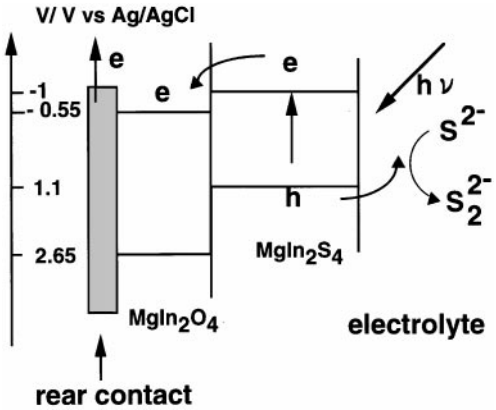

FIG. 5. The schematic diagram of charge generation and injection process of the illuminated $MgIn_2S_4|MgIn_2O_4$ electrode.

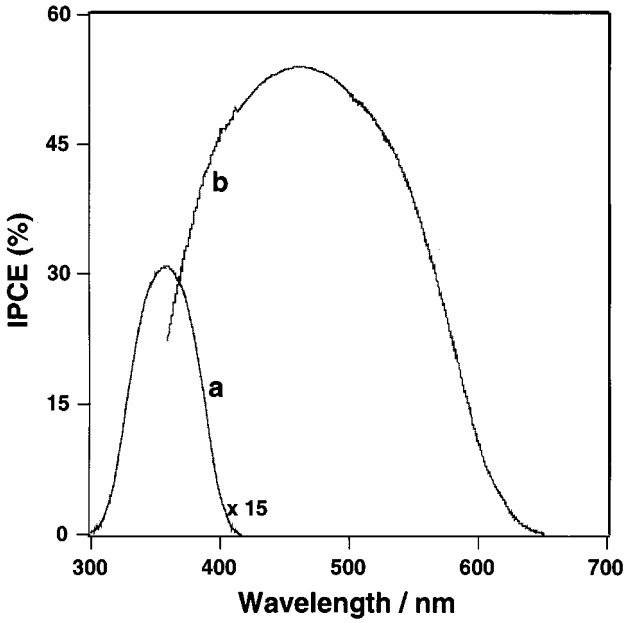

FIG. 6. Variation of incident photon conversion efficiency of (a) Pt|polysulfide|$MgIn_2O_4$, cell and (b) Pt|polysulfide|$MgIn_2S_4|MgIn_2O_4$ PEC cell with wavelength. The electrode was biased at 200 mV vs Ag|AgCl.

Here *e* and *h* represent the photogenerated electron and hole, respectively. Photoinduced electrons in the conduction band of $MgIn_2S_4$ are injected into the conduction band of $MgIn_2O_4$, while photogenerated holes left in the valance band of $MgIn_2S_4$ are quickly consumed to oxidize polysulfide in the electrolyte or oxidize itself (photocorrosion). The energy difference at the interface of two materials prevents reverse flow and/or recombination of charge carriers. Efficient charge separation at the interface via Eq. [3] results in high photocurrent for $MgIn_2S_4|MgIn_2O_4$ electrodes. Proper choice of multicomponent semiconductors might improve performance of semiconductor thin film devices.

In order to further evaluate the cell performance, we measured variation of incident photon conversion efficiency (IPCE) of the cell with wavelength. Variation of incident photon conversion efficiency with wavelength of the $MgIn_2O_4$ electrode before and after sulfurization is shown in Fig. 6. It should be noted that quite high efficiency, up to 50%, is observed at 475 nm for a $MgIn_2S_4|MgIn_2O_4$ electrode. The observed decrease in the photocurrent in IPCE spectra for the $MgIn_2O_4$ electrode and the $MgIn_2S_4|MgIn_2O_4$ electrode in Fig. 6 at shorter wavelengths can be attributed to a higher absorption coefficient of the electrode at shorter wavelengths. Since only a thin layer near the surface of an electrode is excited at short wavelength, electron–hole concentration is high in this thin layer. Therefore, electron–hole recombination occurs efficiently near the surface of an electrode by excitation at a shorter wavelength, which leads to a decrease in the IPCE as shown in Fig. 6 (18). Strong absorption in the UV region by polysulfide may be another reason. Close resemblance of action spectra of $MgIn_2S_4|MgIn_2O_4$ electrodes with diffuse reflectance spectra of $MgIn_2S_4|MgIn_2O_4$ electrodes at the bandgap region prove charge generation by $MgIn_2S_4$. As is shown in Fig. 6, photocurrent of $MgIn_2O_4$ electrodes flows under irradiation with near ultraviolet light at wavelengths shorter than 490 nm. However, for $MgIn_2S_4|MgIn_2O_4$ electrodes, the wavelength of light at which photocurrent follows extends over the whole visible wavelength region from 400 to 700 nm. This result indicates semiconductor sensitization by the $MgIn_2S_4$ layer formed on the $MgIn_2O_4$ substrate. The mechanism of semiconductor sensitization by the $MgIn_2S_4$ layer formed on the $MgIn_2O_4$ substrate is explained well by Eqs. [2] and [3] as well as by the energy diagram in Fig. 5. It is noted that the magnitude of the photocurrent and its quantum efficiency are fairly large in the system, as shown in Figs. 4 and 6. The observed similarities of the action spectra of $MgIn_2S_4|MgIn_2O_4$ electrodes to those of $In_2S_3|In_2O_3$ electrodes (19) may be due to common features of the electronic structure of $MgIn_2S_4$ and In_2S_3. Previous studies have shown that the electronic structure of $CdIn_2S_4$ has some features in common with those of CdS and In_2S_3(20). The variation of the maximum attainable photocurrent of the Pt|polysulfide|$MgIn_2S_4|MgIn_2O_4$ cell as a function of sulfurization time is shown in Fig. 7. As is shown in this figure, photocurrent increases with sulfurization time up to a maximum and then photocurrent decreases with prolonged sulfurization time. This result indicates that thicker $MgIn_2S_4$ on $MgIn_2O_4$ is undesirable for efficient charge separation, probably because increased density of grain boundaries of $MgIn_2S_4$ microcrystals caused by a higher degree of sulfurization enhances recombination of photogenerated electrons and holes. High resistivity ($> 10^4\ \Omega$ cm) was observed on $MgIn_2S_4|MgIn_2O_4$ electrodes with a higher degree of sulfurization, which suggests enhanced density

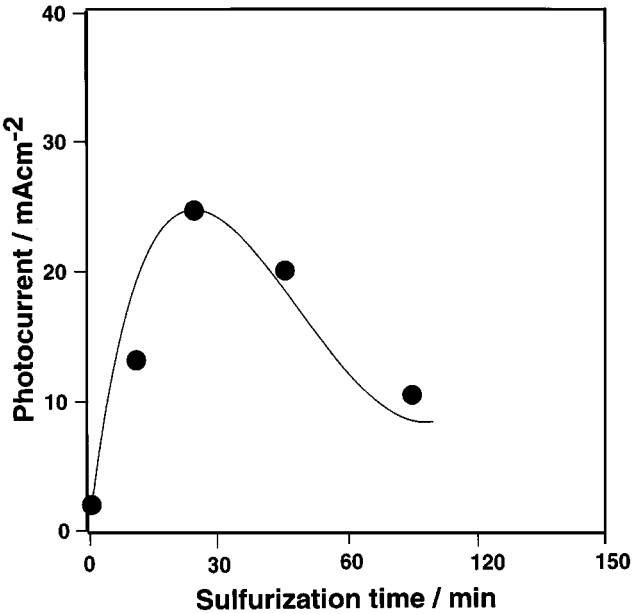

FIG. 7. Variation of attainable maximum photocurrent of a Pt|polysulfide|$MgIn_2S_4$|$MgIn_2O_4$ cell as a function of sulfurization time under illumination with polychromatic light (250 mW cm^{-2}). H_2S gas was passed at a constant rate of 0.5 ml/min throughout the sulfurization. The electrode was biased at 200 mV vs Ag|AgCl.

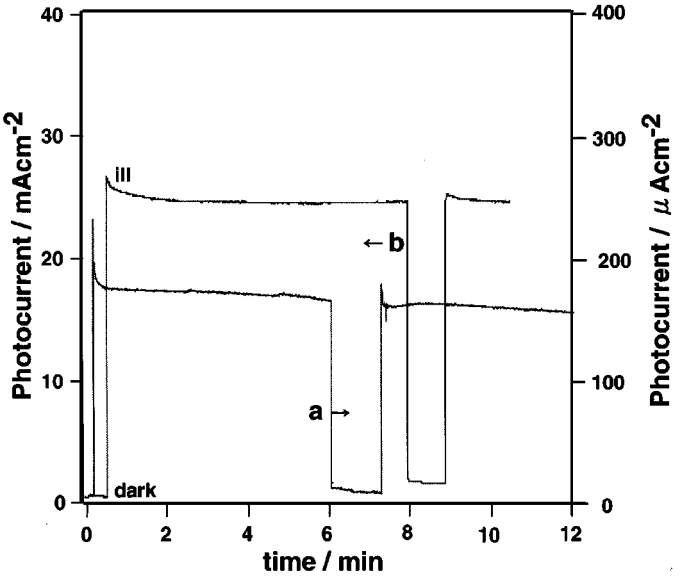

FIG. 8. Variation of the short-circuit photocurrent of (a) Pt|polysulfide|$MgIn_2O_4$ cell and (b) Pt|polysulfide|$MgIn_2S_4$|$MgIn_2O_4$ cell as a function of time under illumination with polychromatic light (250 mW cm^{-2}). The electrode was biassed at 200 mV vs Ag|AgCl.

of the grain boundaries due to prolonged sulfurization. This might be a reason less photocurrent was observed on $MgIn_2S_4$|$MgIn_2O_4$ electrodes with higher degree of sulfurization. The variation of short circuit photocurrent of Pt|polysulfide|$MgIn_2S_4$|$MgIn_2O_4$ cell as a function of time is shown in Fig. 8. As is shown in Fig. 8, initially the Pt|polysulfide|$MgIn_2S_4$|$MgIn_2O_4$ cell exhibited slow decay in photocurrent with time illumination. This photocurrent decay is thought to be caused by photocorrosion of $MgIn_2S_4$. Similar photocorrosion has been generally observed on other metal chalcogenide elctrodes in various electrolytes (19,21). Photocurrent decay limits practical application of $MgIn_2S_4$|$MgIn_2O_4$ electrodes in solar cells. Further studies would be necessary to solve this problem. The dark current enhancement of Pt|polysulfide|$MgIn_2S_4$|$MgIn_2O_4$ cell may be attributed to deterioration of $MgIn_2S_4$ surface by photocorrosion under illumination.

4. CONCLUSION

$MgIn_2O_4$ was prepared from the solid state reaction of MgO and In_2O_3. $MgIn_2O_4$ exhibited a high degree of thermal stability. Sulfurization extended the photoresponse of $MgIn_2O_4$ toward the visible region. The bandgap of $MgIn_2S_4$ was evaluated as 2.1 eV. Significantly enhanced anodic photocurrent was observed on $MgIn_2S_4$|$MgIn_2O_4$ electrodes. Efficient charge separation in $MgIn_2S_4$|$MgIn_2O_4$ electrodes at the interface of $MgIn_2S_4$ and $MgIn_2O_4$ had a favorable influence on the performance of the cell.

ACKNOWLEDGMENTS

One of the authors, P.M.S., thanks T. Otake, O. Okawa, and K. Hamaya for various help. Financial support by the Ministry of Education, Sports, Science, and Culture in Japan (MONBUSHO) is greatly acknowledged by P.M.S.

REFERENCES

1. B. O'Regan and M. Gratzel, *Nature* **353,** 737 (1991).
2. R. Dabestani, A. J. Bard, A. Camton, M. A. Fox, T. E. Mallouk, S. E. Webber, and J. M. White, *J. Phys. Chem.* **92,** 1872 (1988).
3. A. J. McEvoy and M. Gratzel, *Sol. Cells Sol. Energy Mater.* **32,** 221 (1994).
4. R. Vogel, K. Pohl, and H. Weller, *Chem. Phys. Lett.* **174,** 241 (1990).
5. M. Ashokkumar, A. Kudo, N. Saito, and T. Sakata, *Chem. Phys. Lett.* **229,** 383 (1994).
6. Y. Yaski, N. Sonoyama, and T. Sakata, *J. Electroanal. Chem.* **469,** 116 (1999).
7. Di Liu and P. V. Kamat, *J. Electroanal. Chem.* **347,** 451 (1993).
8. D. Fiorani and S. Viticoli, *Solid State Commun.* **32,** 889 (1979).
9. L. Gastaldi and A. Lapiccirella, *J. Solid State Chem.* **30,** 223 (1979).
10. H. Kawazoe, N. Ueda, H. Unno, T. Omata, H. Hosono, and H. Tanoue, *J. Appl. Phys.* **76**(12), 7935 (1994).
11. K. L. Chopra, S. Major, and D. K. Pandya, *Thin Solid Films* **102,** 1 (1983).
12. N. Ueda, T. Omata, N. Hikuma, K. Ueda, H. Mizoguchi, T. Hahimoto, and H. Kawazoe, *Appl. Phys. Lett.* **61**(16), 1954 (1992).

13. C. W. W. Hoffman and J. J. Brown, *J. Inorg. Nucl. Chem.* **30,** 63 (1968).
14. N. N. Nifriev, *Solid State Commun.* **92**(9), 781 (1994).
15. F. Cerrina, C. Quaresima, I. Abbati, L. Braicovich, P. Picco, and G. Margaritond, *Solid State Commun.* **33,** 4229 (1980).
16. J. B. Goodenough, *J. Phys. Chem. Solids* **30,** 261 (1969).
17. R. Memming, *Top. Curr. Chem.* **143,** 81 (1988).
18. K. Vinodgopal, U. Stafford, K. A. Gray, and P. V. Kamat, *J. Phys. Chem.* **98,** 6797 (1994).
19. P. M. Sirimanne, S. Shiosaki, N. Sonoyama, and T. Sakata, *Solar Cells Solar Energy Mater.*, in press.
20. H. Ihara, H. Abe, S. Endo, T. Irie, *Solid State Commun.* **28,** 563 (1978).
21. D. J. Arent, H. D. Rubin, Y. Chen, and A. B. Bocarsly, *J. Electrochem. Soc.* **139,** 2705 (1992).